12

Asian Dust Storm as a Natural Source of Air Pollution in East Asia; its Nature, Aging, and Extinction

Chang-Jin Ma
Fukuoka Women's University
Japan

1. Introduction

Asian dust–storm (hereafter called "ADS") often occurred at desert and loess areas in northwest of China traverse China continent and can be extended to Pacific Ocean passing through Korea and Japan in every spring time. This dust is blown up by strong wind behind the cyclone and delivered in free troposphere by westerly jet. Even though ADS is a peculiar phenomenon occurred in China continent, this ADS have led to the significant environmental change in East Asia and North Pacific ocean for a long time. A new theory states that dust storms might deflect sunlight, thus slowing down climate change. However, there is growing proof that dust storms are a health hazard. Dust clouds harbour viruses, fungi and bacteria as well as heavy metals and other pollutants.

Although ADS can cause many disasters, it is said that ADS make a contribution to the neutralization of acid rain caused by consumption of a large amount of fossil fuels. This ADS finally dissipates when the particles are removed from the atmosphere by dry and wet removal processes. Gravitational settling of large particles (>10 μm) occurs near the source within the first day of transport. Wet removal occurs sporadically throughout the 5-10 day lifetime of the remaining smaller size dust particles.

Here, the special information on ADS particles which is a peculiar natural source of air pollution in East Asia and the Pacific Ocean is reported.

2. Physicochemical properties of ADS sources

Numerous studies on the ADS particles have been performed and reported (Braaten et al., 1986; Darzi et al., 1982; Duce et al., 1980; Iwasaka et al., 1988; Lafon et al., 2004; Ma et al., 2004c; Song et al., 2006; Song & Carmichael, 1999; Zhang et al., 2003). It is presumed that the chemistry of ADS particles can be influenced by absorption of atmospheric gases and subsequent oxidation of the absorbed gases on the surface during long-range transport. It is however desirable to explain how man-made pollutants and sea-salt aerosol react with natural ADS particles. In order to understand these denaturations of ADS particles, information of the nature of original sands at the local source areas is prerequisite.

However, unfortunately, relatively little is known about the individual dust sands in various source regions (Nishikawa et al., 2000).
The primary goal of this section is to report the comparative characteristics of the original sands collected at four different desert regions in China.

2.1 Experimental methods

2.1.1 Description of sampling sites and sampling method of desert sands

The sedimentation of the whole gigantic particles (e.g., larger than 10 μm) happens near the source region of dust storm (Husar et al., 2001). It is a generally acknowledged fact that Taklimakan desert, which is a long way off from receptor areas, does not exert much impacts on receptor areas. In light of this, four desert areas (Yinchuan, Wuwei, Dulan, and Yanchi) located nearby Gobi desert were chosen in the present study (see Fig. 1).

Fig. 1. Map showing the desert areas of sand collection

Yinchuan lies in the middle of the Yinchuan or Ningxia Plain. It is sheltered from the deserts of Mongolia by the high ranges of the Helan Mountain on its west. Yinchuan has a temperate continental climate with an annual average temperature of 8.5 °C, with 158 frost-free days. Its annual rainfall averages 200 mm. Wuwei is situated in the central part of

Gansu province, on the east end of Hexi Corridor. Wuwei has a temperate semiarid climate with an annual average temperature of 8.7 °C, with frost free period of 165 days and annual precipitation of 158 mm. Dulan County belongs to West Lake Mongolia & Tibetan Autonomous prefecture, Qinghai Province. The mean annual temperature is 3 °C with a January average of -10 °C and a July average of 15 °C, and the mean annual precipitation is 188 mm, 78% of which falls from May through September. Yanchi lies in the semi-deserts of the arid north west. There is less rain but more wind all the year round, and weather is extremely dry. The mean annual temperature is 9.2 °C (-7 °C (January) to 20.4 °C (July)) with mean annual precipitation of 225 mm (Li et al., 2007).
To obtain a representative sand sample, three different points (within a 500 m radius) were selected separately and randomly for each desert. A spade which is one of common tools used to sample soil was applied to collection of surface sands.

2.1.2 Chemical identification

The same amounts (2 g of dried sands) of desert sands collected among three different points were evenly mixed. The mixed desert sands were dissolved in 20 ml of pure deionized water and mixed in an ultra-sonicator for 20 min. After ultrasonic extraction, the sample was allowed to be filtered through the **Nuclepore**® filter with a 0.2 μm pore size.
To determine the elemental concentration, both soluble and insoluble fractions of sands were submitted for Particle Induced X-ray Emission (PIXE) installed in Quantum Science and Engineering Center, Kyoto University. Since the self-absorption of emitted characteristic X-ray can occur when specimens are thick, the insoluble solid sands were pulverized and homogenously deposited onto a polycarbonate substrate film. Then they were irradiated by the proton beam of PIXE system. Due to analytical difficulties with the liquid samples by PIXE, a 20 μl water soluble fraction was mounted on a polycarbonate substrate film and dried under infrared lamp. PIXE analysis was performed with a proton beam of 6 mm diameter and 2.0 MeV energy from a Tandem Cockcroft. Beam intensities of 10 to 60 nA were employed with the total dose of about 20 μC. X-ray with the energy of 14.8 keV emitted from the target was detected by a Si (Li) detector which had a resolution of 152 eV at 5.9 keV. The more detailed analytical procedures and experimental set-up used for PIXE analysis have been described elsewhere (Ma et al., 2001).
To analyze the chemical structure and mixing state of surface and inner individual sands, X-ray fluorescence (XRF) microprobe system equipped at Super Photon ring 8 GeV (SPring-8) BL37XU was applied. Hayakawa (2000) established this BL-37XU at SPring-8 that allows chemical analysis for a wide variety of specimens. This method has been successfully used to carry out the reconstruction of elemental map with the quantification of multiple elements at femto gram level sensitivity (Hayakawa et al., 2001). More details about the analytical procedures and experimental set-up for XRF microprobe analysis can be found in Hayakawa et al. (2001).

2.2 Results and discussion

2.2.1 Morphology, color, and size distribution

The morphology of original desert sands collected from four different desert areas was displayed in Fig. 2. Nearly all of sands have irregular shape with yellowish coloration, whereas some sands show peculiar colors such as bluish, blackish, and reddish. Minerals are colored because certain wavelengths of light are absorbed. It is suggested that this color dissimilarity is influenced largely by chemical composition and atomic structure of the mineral.

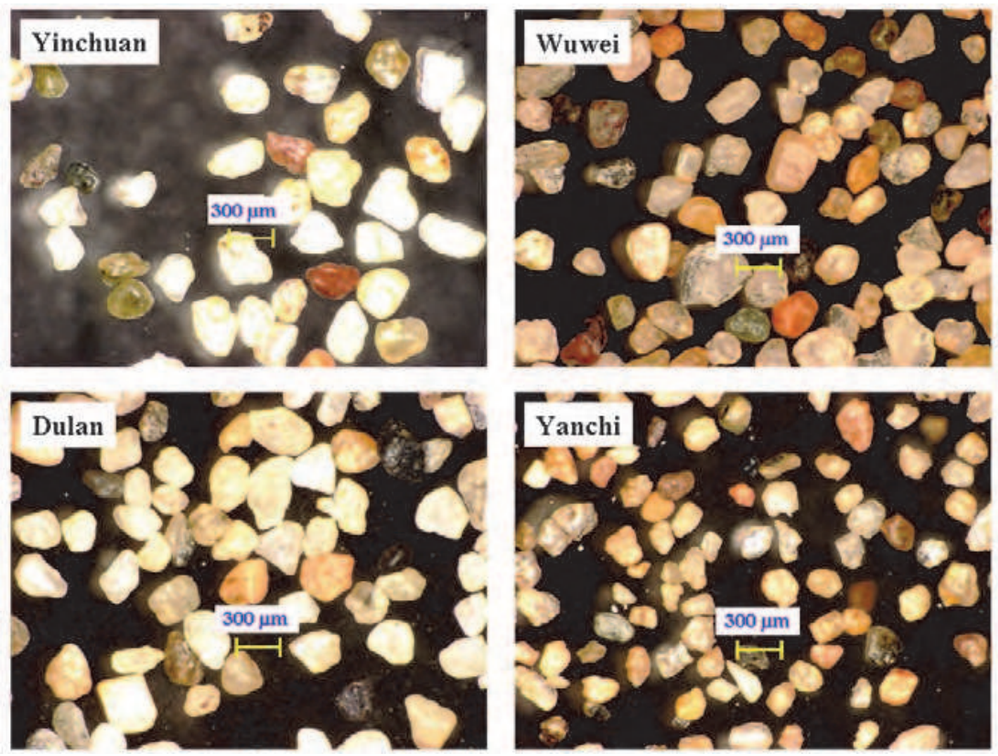

Fig. 2. Microscopic image of sands collected at four desert areas in China (x100)

The shape of size distribution for sands collected at Yinchuan, Wuwei, and Dulan sites is monomodal to show the maximum level between 200 and 300 μm. On the other hand, the maximum level for Yanchi desert sands is displayed between 100 μm and 200 μm. The size of sands at Wuwei desert area is relatively wide spread in the range up to 600 μm.

2.2.2 Chemical properties of bulk and individual sands

In order to conduct quantitative elemental analysis, the masses of deposited sand powders onto polycarbonate substrate film have to be precisely measured. However, due to the small amount of pulverized sands homogenously mounted onto polycarbonate substrate film, it is not possible to conduct mass measurement. Hence, the concentration ratios of Z/Si are listed for soluble and insoluble fractions of the four kinds of desert sand in Table 1. Here, the concentration ratios of Z/Si were calculated by the initial result (μg cm^{-2}) of PIXE analysis. As might be expected, there is a tendency towards higher Z/Si ratios for soil derived elements such as : Si>Fe>K>Ca at Yinchuan, Si>K>Fe>Ca at Wuwei, Si>Ca>Fe>K at Dulan, and Si>Ca>K>Fe at Yanchi. Unfortunately, Al concentration cannot be reliably determined by our PIXE system. Although it has negligible ratio, S was detected in insoluble fraction of Wuwei sample with 0.0003 S/Si ratio and soluble fraction of Dulan sample with 0.0282 S/Si ratio. In addition, Cl was contained in every desert sand with the exception of the insoluble portion of Yanchi area. As reported by Mason (1966), some crustal rocks (such as shale and limestone) contain S and Cl. Therefore one should give attention to data interpretation about the aging processes of dust particles with sea-salts and man-made S. The relative elemental ratios summarized in Table 1 can be a means to assess the transformation of dust particles during long-range transport and other aging processes.

	Insoluble fraction				Soluble fraction			
	Yinchuan	Wuwei	Dulan	Yanchi	Yinchuan	Wuwei	Dulan	Yanchi
Si	1.0000	1.0000	1.0000	1.0000	1.0000	1.0000	1.0000	1.0000
S	N.D.[a]	0.0003	N.D.	N.D.	N.D.	N.D.	0.0282	N.D.
Cl	0.0008	0.0017	0.0036	0.0027	0.0386	0.0281	0.0404	N.D.
K	0.0530	0.0878	0.0761	0.1009	0.2231	0.1569	0.1818	0.1693
Ca	0.0473	0.0239	0.7011	0.2116	0.5063	0.3132	0.9620	0.3488
Ti	0.0035	N.D.	N.D.	N.D.	N.D.	N.D.	N.D.	N.D.
V	0.0042	0.0032	0.0076	0.0044	0.0000	0.0060	0.0107	0.0105
Cr	0.0015	0.0010	0.0056	0.0024	0.0077	0.0037	0.0098	0.0064
Mn	0.0046	0.0019	0.0072	0.0050	0.0100	0.0085	0.0176	0.0174
Fe	0.1666	0.0506	0.2077	0.0988	0.3682	0.3208	0.4007	0.4345
Cu	0.0018	0.0008	0.0022	0.0008	N.D.	N.D.	0.0063	0.0066
Zn	0.0011	0.0004	0.0017	0.0008	N.D.	N.D.	0.0036	0.0021
Sr	0.0014	0.0012	0.0027	0.0012	N.D.	N.D.	0.0081	0.0030
Pb	0.0003	0.0002	0.0008	0.0004	0.0059	0.0023	0.0025	0.0008

[a] Non-Detected.

Table 1. The concentration ratios of Z/Si for four kinds of desert sands as a function of water solubility

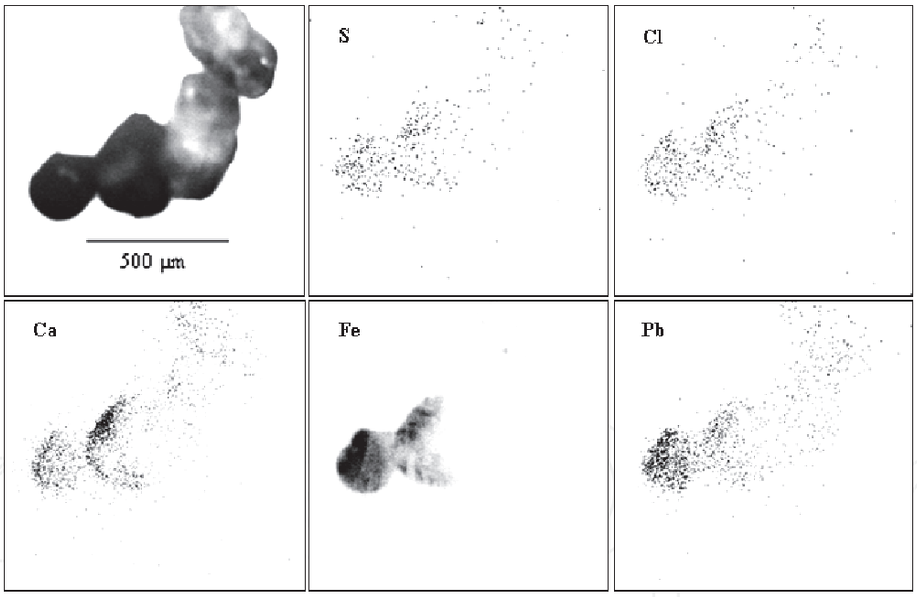

Fig. 3. The reconstructed XRF elemental maps corresponding to individual sands collected in at Yinchuan desert area

An example of XRF elemental maps and microscopically imaged desert sands (top left) collected at Yinchuan desert area in China are presented in Fig. 3. It was possible to draw the distribution of components in and/or on desert sands. From XRF elemental maps, it can be visually confirmed that S, Cl, and Pb were present overall sand surface as the minor components. In contrast, Fe distribution is partially concentrated on sand surface. However, the elemental distribution on sand surface can be influenced by the degrees of an angle between Si (Li) detector recording the fluorescence X-rays and sample holder.

3. Chemical transformation of individual ADS particles

During long-range transport of air masses containing ADS particles over oceans, ADS particles can capture gases or coagulate solid particles and react with each other, leading to a change in chemical compositions (Duce et al., 1980; Hwang et al., 2008; Iwasaka et al., 1988; Ma et al., 2004c; Nishikawa and Kanamori, 1991). Zhang et al. (2003) made an investigation for the elemental composition and size of individual ADS particles and their mixture state with sea salt, sulfate, and nitrate. They reported that about 60-85% of dust particles collected at southwestern Japan was internally mixed with sea salt. Chemical transformation of ADS particles can alter the marine ecosystem and radiative properties of dust clouds (Zhang and Iwasaka, 1998). Hwang et al. (2008) reported that ADS particles were mixed with sea-salts entrained over the Yellow Sea, as well as air pollutants from the eastern China coastal areas.

Microbeam Particle Induced X-ray Emission (PIXE), often called micro-PIXE, is a variation of PIXE that has become very important in recent years. It is a combination of the microbeam technique with PIXE analysis (Johansson and Campbell, 1988). By using micro-PIXE analytical system, Ma et al. (2000) carried out the single particle analysis for the coarse particles collected in an ADS event. In doing so, they pointed out that the significant Cl was detected in individual dust particles. However, they did not fully discuss the internal mixing state in view of reaction between dust particles and sea-salts. Because other Cl sources such as gaseous Cl and non sea-salt particulate Cl can also influence on the aging processes of ADS particles (Ma et al., 2008). Hence, in order to clearly discuss the mixing processes of ADS particles with sea-salts from micro-PIXE data, one should simultaneously analyze Na in individual ADS particles that were captured at receptor area. However unfortunately, as mentioned above, until now light elements including Na have not been determined by micro-PIXE. Broadening the range (including $Z<14$) of analyzed elements by micro-PIXE is urgently needed to assess the aging processes of ADS particles.

In the present work, an attempt was made to broaden the range of analyzed elements by employing the double detector system at micro-PIXE. This section shows the preliminary results of the double detector system and its application to the interpretation of the mixing state of individual ADS particles with sea-salt.

3.1 Experimental methods

3.1.1 Sampling of ambient ADS particles

An intensive measurement of ambient ADS particles was performed at a ground-based site in Fukuoka, Japan (33.40^{o}N; 130.26^{o}E) on April 20, 2005. Because of its closeness to the Asian mainland, this area can be directly exposed to the outflow of air masses from the Asian continent during springtime.

For the sampling of ambient ADS particles, a low pressure Andersen impactor (LPAI) samplers (Tokyo Dylec Co., LP-20) was operated on April 20 (12:00-15:00), 2005. As one of multi-stage particle sampling instruments, this LPAI with multi-orifice was designed to measure the size distribution and mass concentration of particulate matter. Particles are sampled directly on substrate material (80 mm diameter Nuclepore® filter) arranged behind the jet-nozzles of an impactor. The detailed cut-off particle diameter of each stage for the LPAI was already mentioned in other papers by Ma et al. (2004a) and Ma and Kim (2008). During the sampling period, the ranges of temperature and relative humidity (RH) were 18.8-21.7 ^{o}C and 41-56%, respectively.

3.1.2 The novel double detector system of micro-PIXE

Table 2 indicates the properties of double X-ray detectors. The HP-Ge X-ray detector has moderate energy resolution and poor detection efficiency below 2 keV because of its Ge L-shell absorption edge and backscattering proton absorber (60 μm thick polypropylene). The Si(Li) X-ray detector was set at a symmetrical position with the HP-Ge X-ray detector with respect to the beam axis. The energy resolution of the Si(Li) detector is excellent, and this higher energy resolution results in a better signal-to-background ratio and smaller peak overlapping, especially in the low-energy regions. The detector window is 8 μm-thick Be and attached with an annular type absorber (100 μm-thick Mylar) with a center hole (3 mm in diameter). This Si(Li) detector can finally provide a fairly good detection efficiency for X-rays below 2 keV. Details of this double X-ray detectors system for PIXE Analysis have been described elsewhere (Sakai et al., 2005).

X-ray detector	Model	Window ( )[b]	Absorber	Distance[c]	Prioty element	Detectable elements
HP[a]-Ge	IGLET-X-11145	Be (25 μm)	Polypropylene 60 μm	22 mm	Middle-Heavy	≥ Si
Si(Li)	LS30135	Be (8 μm)	Mylar 100 μm	18 mm	Light	≥ Na

[a]High-purity

[b]Thickness

[c]Detector - window distance

Table 2. Specification of two different X-ray detectors

3.2 Results and discussion

Fig. 4 shows the micro-PIXE elemental spectra for the seven arrow-marked individual ADS particles that were collected on the 2nd stage (5.07 μm aerodynamic diameter) of LPAI.

Outer blackly filled and inner greyly filled spectra were formed by scanning the whole area retaining seven particles (a blackly filled square at right side of Fig. 4) and each indicated particle, respectively. The scanning of microbeam on each individual particle enabled us to draw more clearly separated peaks of each element including light elements (e.g., Na, Mg, and Al). First of all, the micro-PIXE spectra displayed in Fig. 4 shows a severe particle-to-particle variation of the elemental composition among individual coarse particles collected during our intensive field measurement campaign. From the inner greyly filled spectra, individual particles can be classified into two distinct groups (i.e., above four particles (group 1) and below three particles (group 2) groups). In the particles belonged to group 1, Na and Cl coexist with soil-derived components such as Al, Si, K, Ca, and Fe. The particles of group 1 are the typical example of internally mixed particles which contain a uniform mixture of components from each of the sources. The coexistence of sea salt and mineral components also indicates that ADS particles were experienced aging processes namely, chemical transformation, in the course of their long-range transport. Whereas, only marine components (e.g., Na, Cl, S, and Mg) were detected in the particles of group 2.

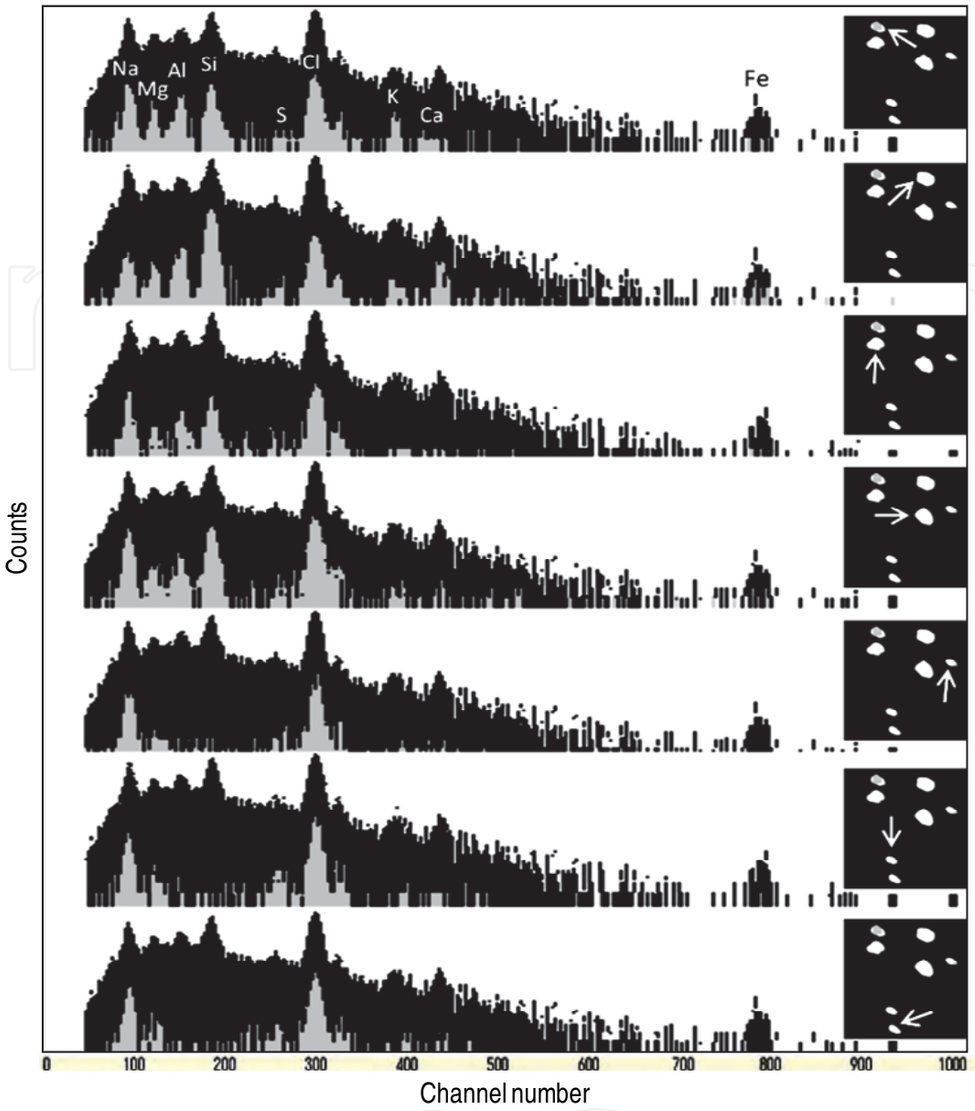

Fig. 4. Micro-PIXE elemental spectra for individual ADS particles collected on the 2nd stage (5.07 μm aerodynamic diameter) of LPAI

Fig. 5 displays an example of micro-PIXE elemental maps taken on two particles (5.07 μm aerodynamic diameter) collected during ADS event. Two combined masks of total elements are schematically shown on the last insert.

The particle displayed at top portion of scanning area is containing marine components (e.g., Cl, Na, and S). Whereas, several crustal elements (e.g., Si, Al, and Ca) are principally distributed in and/or on a particle located at bottom of scanning area. On the other hand, Mg and Ca, which are minor (or relatively minor) composition in both sea-salt (Mg: 0.128 wt.% and Ca: 0.0418 wt.%) and dust sand (Mg: 1.57 wt.% and Ca: 5.83 wt.%) (The standards of China loess and Simulated Asian mineral dust, 1998) are weakly coexisting in and/or on two particles. From this elemental map and mask replayed corresponding to individual two particles we can reasonably suggest that two particles are externally mixed particles (i.e., each particle arises from only one source).

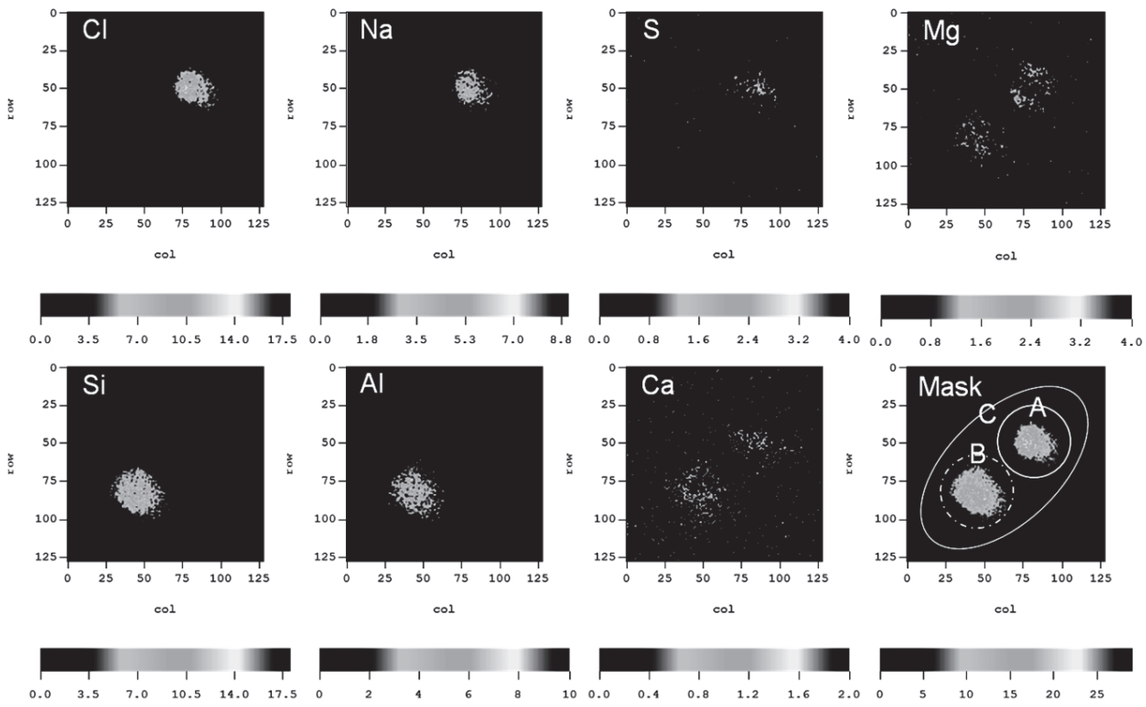

Fig. 5. An example of micro-PIXE elemental maps taken on two particles collected during ADS event. Scanning area of microbeam is 25×25 μm²

Micro-PIXE analysis has the scanning ability of microbeam with a 1-2 μm beam spot size. By scanning this microbeam, we can obtain spatial distribution of trace elements in individual particles. As a result, it is possible to know the portion-to-portion variation of elemental compositions in a particle. Fig. 6 shows an example of the micro-PIXE elemental spectra for two different portions of an ADS particle with 5.07 μm aerodynamic diameter. Outer white and inner black spectra were formed by scanning the whole and each square portion on a particle, respectively. According to this analytical result, the top portion of particle contains both sea-salt and silicon. However, only sea-salt components were detected in the bottom portion of particle. It can therefore be said that the chemically transformed ADS particle shows heterogeneous elemental distribution. This heterogeneous elemental distribution in an ADS particle might be caused by two dissimilar aging processes (i.e., (a): collision (or coagulation) of dust particles and sea-salts and (b): in-cloud scavenging of both particles). The modification of ADS particles occurred most probably due to the collisions and coagulations of dust particles and sea-salts (Zhang and Iwasaka, 2004). Zhang and Iwasaka (2004) suggested that the interaction of ADS particles and sea-salt is an important process in size and compositional changes of ADS particles during their long range transport, consequently affecting mass transformation and optical properties in the atmosphere. Moreover, a cloud formation process contributes significantly to the chemical modification of ADS particles (Ma et al., 2004b). From the study on individual cloud droplets by an X-ray fluorescence microprobe analysis, Ma et al. (2004b) reported that a large number of crustal particles were incorporated into cloud droplets during their long-range transport.

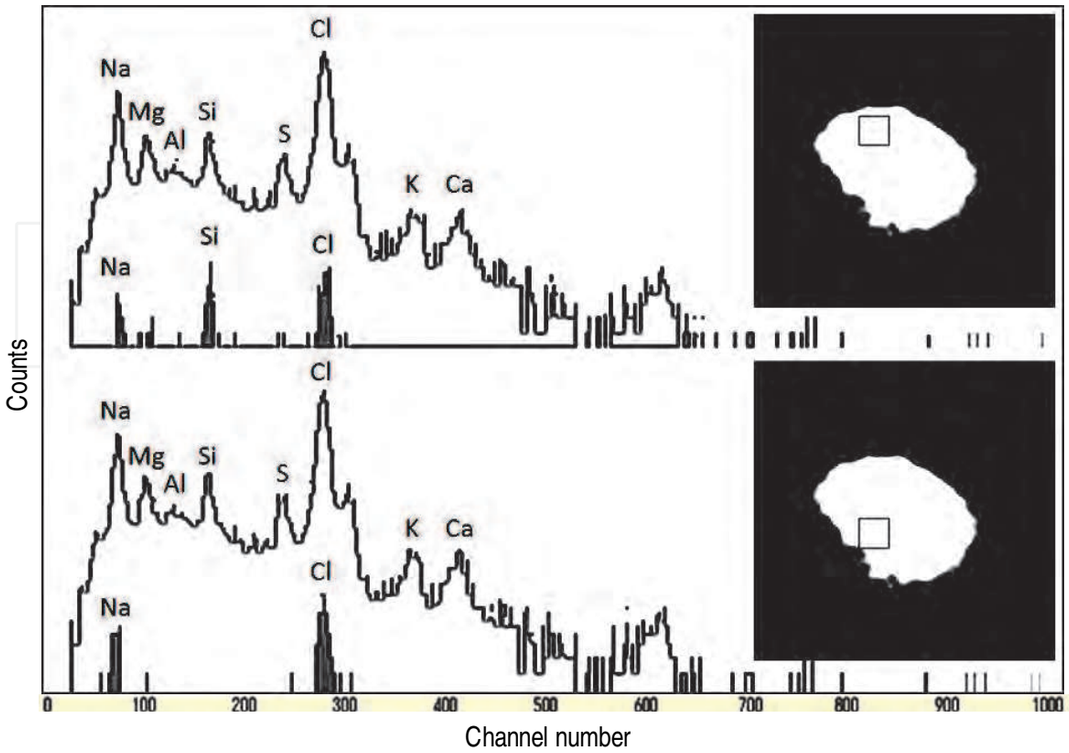

Fig. 6. Micro-PIXE elemental spectra for two different portions of an ADS particle

Fig. 7 illustrates a presumable explanation for the transformation processes of the ADS particles with sea-salt by heterogeneous nucleation. Two types of transformation processes of the ADS particles can be identified, i.e., the coalescence of two different droplets formed by heterogeneous nucleation on a separated ADS particle and a sea-salt and ((a) of Fig. 7) and the collision of an ADS particle to the droplet formed by a sea-salt nucleation ((b) of Fig. 7). Although ADS particles are insoluble in water, they begin to serve as centers with the condensation of water vapor. ADS particles are less soluble than marine of anthropogenic aerosols, their solubility weathered by condensation-evaporation cycles can be increased (Desboeufs et al., 2001). In addition, these homo/heterogeneous nucleation processes can be homomolecular (involving a single species) or heteromolecular (involving two or more species) (Desboeufs et al., 2001). According to the transformation processes of the ADS particles with sea-salt (as illustrated in Fig. 7), the possible reasons of portion-to-portion dissimilarity shown in Fig. 6 (i.e., (a) upper scanned portion: Na, Si, and Cl and (b) below scanned portion: Na and Cl) of elemental distribution on and/or in an ADS particle can be potentially evaluated by below three aging processes of the ADS particles.

As the first aging process ((a) of Fig. 7), both ADS and sea-salt particles were transferred into different cloud droplets via nucleation scavenging. This in-cloud scavenging of particles is called rainout. During this rainout processes, sea-salt particles were perfectly melted; however, hydrophobic ADS particle were keeping a horizontal water film on its surface (Desboeufs et al., 2001). Both cloud droplets were then consolidated, when they grew and diffuse in cloud layer. Finally, descending air parcel by high pressure and evaporation of water from cloud droplet made a new particle which contained partially sea-salt crystal on its surface.

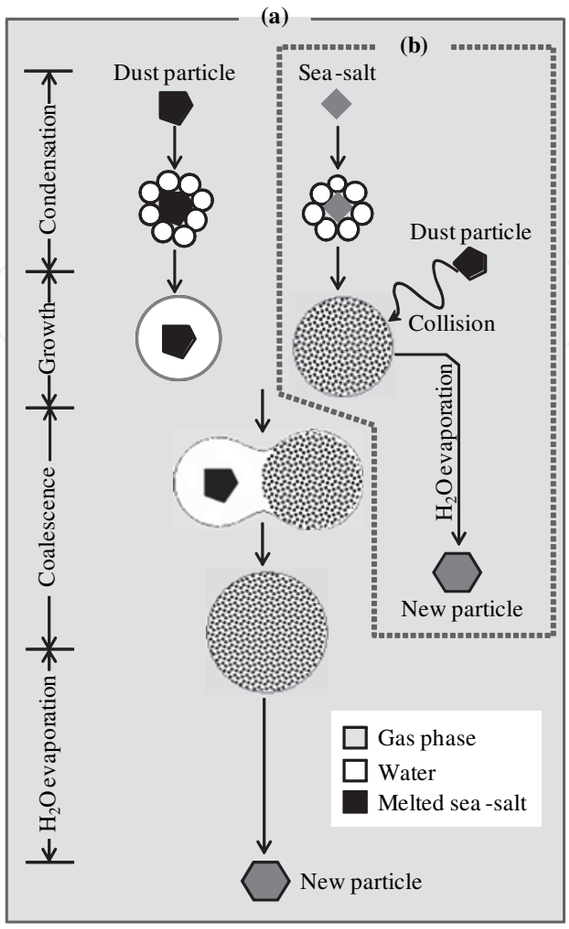

Fig. 7. An illustrative explanation of the transformation processes of the ADS particles with sea-salt via nucleation scavenging

As the second aging process ((b) of Fig. 7), an ADS particle that did not take up any water (i.e., it cannot be dissolved in cloud droplet by itself) was scavenged by a cloud droplet (i.e., through collision) formed by rainout of sea-salt. Then a chemically different particle was born. As distinct from nucleation scavenging, the collisions and coagulations of an ADS particle and a sea-salt can be thought as the third aging process. This homogeneous particle-to-particle reaction is probably due to the modification of ADS particle.

4. Removal of ADS particles by rainout and washout

If the relative humidity of the air parcel reaches a critical humidity, the value of which depends on the size and chemical composition of the aerosol present, the droplets become activated, grow freely by water vapor diffusion, and cloud droplets are formed. This in-cloud scavenging of particles is called rainout. Cloud and precipitation contribute significantly to the removal of Asian dust storm particles from the atmosphere (Ma et al., 2004). Numerous studies including laboratory, field, and model simulation have been carried out to determine the chemical composition of rain and the scavenging efficiency of aerosol particles by raindrops (Baez et al., 1995; Chate & Kamra, 1997; Hallberg et al., 1997).

Since the chemical content of raindrops is variable according to the mechanisms such as condensation nuclei inside clouds, pollutant scavenging, collision, coalescence and break-up of falling raindrops, and evaporation, chemical processes in the atmosphere as the washout of particles and gases are not sufficiently described by the usual determination of elemental concentration in rain water (Ma et al., 2001; Tenberken & Bächmann, 1996). Since the analysis of rain as bulk phase will lead to a loss of detailed information, the sampling and analysis of individual and size-classified raindrops must be performed (Tenberken & Bächmann, 1996; Ma, 2001). In recent years, Ma's "Collodion-film replication technique" (Ma, 2001) has provided a new method by which chemical analysis of individual raindrops can be carried out. Tenberken and Bächmann 4) applied the capillary zone electrophoresis method to the analysis of a single droplet.

Avila and Rodà (1991) introduced the red rain. The red rain, rain event carrying dust from Sahara desert, North African sources, are frequently falling with average frequency of around 3 events per year at Barcelona and surroundings in NE Spain 8). Red rains show a high load of dissolved ions (Rodà et al., 1993) and particulate matter (Berganetti et al., 1989).

In Japan, a yellow rain, which is rain colored yellow by particulate matter with high pH value (6.35) due to the alkaline dust storm particles, was reported in the end of Mar. 2000 (Ma et al., 2002).

The purpose of this section is to introduce the physiochemical properties of the individual cloud base droplets collected in the western Japan during ADS event. Also the elemental masses in size-classified raindrops collected on the yellow rainfall event were theoretically and experimentally compared.

4.1 Scavenging of ADS particles by cloud droplet

4.1.1 Sampling and analysis of individual cloud droplets

The sampling of individual cloud droplets was carried out at the Kyoto Prefectural acid rain monitoring site (200 m elevation) in the range of Mt. Taiko and the summit of Mt. Taiko (683 m elevation) on the west coast of Japan, respectively during dense Asian dust storm event on 22 Mar. 2002. These mountainous sampling sites (35.37^{o} N, 135.81^{o} E) are located at Yasaka in the north part of Kyoto Prefecture, Japan. This mountainous sampling site is not only a clean region without local pollution sources, but also a geographically advantageous position where can be directly exposed to ADS in some cases. The summit of Mt. Taiko was exposed by cloud during dense Asian dust storm event. For the collection of individual cloud droplets, the replication technique introduced for sampling of individual drizzle droplet by Ma et al. (2001) was applied. About 200 µl of collodion solution (3%) is mounted onto a 47 mm diameter non-hole Nuclepore® filter just before exposure to cloud. When cloud droplets adhere freely onto the thin layer of collodion film (130±10 µm) they gently settled without bounce-off. This procedure not only allows us to get information about the physical properties of droplets but also enable us to analyze the retained components in and/or on cloud droplet. During sampling periods the temperature was ranged from 9.5 ^{o}C and 11.4 ^{o}C and the average relative humidity was around 100%. About 500 separated individual cloud droplets were collected on 20 sheets of collodion film at cloud base level.

In order to characterize the chemical nature of solid residual particles retained in individual cloud droplets, the X-ray microprobe system equipped at SPring-8 BL-37XU was applied.

The analytical procedures and experimental set-up used for XRF microprobe analysis were already mentioned.

4.1.2 Replication of individual cloud droplets

Droplets, unlike dust particles, are unstable. Any contact with a solid surface or another droplet makes the droplet disappear as an entity. Therefore, unlike dust particles for example, droplets cannot be collected on a filter paper for subsequent physicochemical analysis in the laboratory. Also it is difficult to collect cloud as individual droplets because a single cloud droplet has a tiny volume. From this point of view, collodion film method can be one of profitable methods for the study on the physical characteristics as well as for subsequent chemical analysis of individual droplets. The replicas of individual cloud droplets were formed separately on the thin collodion film as shown in Fig. 8.

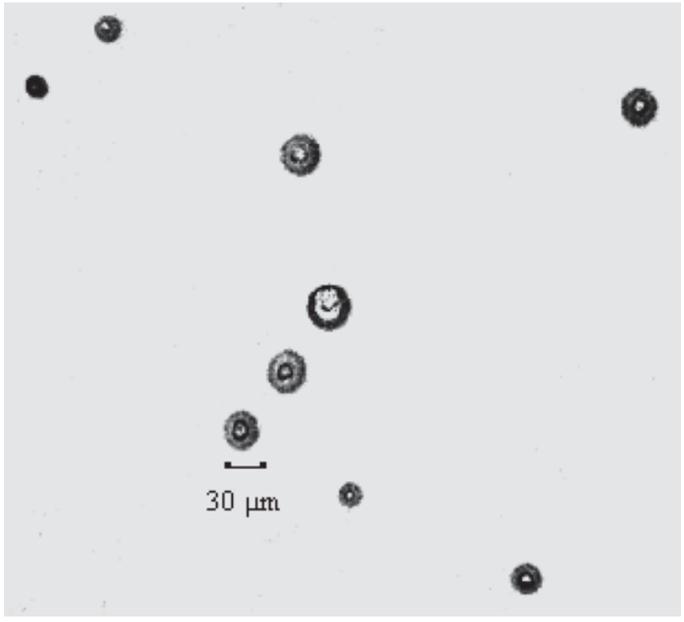

Fig. 8. Replicas of individual cloud droplets formed on collodion film

4.1.3 Chemical properties of residuals in individual cloud droplets

The droplet residues consisted of crustal components were reconstructed as elemental maps. Fig. 9 shows the four kinds of XRF elemental maps of dry residuals in individual cloud droplets. Each elemental map size is 750 μm × 750 μm. Large amount of cloud droplets containing Ca are present on this mapping area (lower left panel). In addition, as a one of substantial fractions of the droplet residues, map of Zn was drown at right upper of Fig. 9. We cloud find the significant distribution of crustal components on the maps of residual particles in individual cloud droplet. This cleanly indicates that a large number of crustal particles were incorporated into cloud droplets during their long-range transport. In other words, soil particles with high amounts of insoluble fractions had high scavenging efficiencies by rain out mechanisms. These XRF elemental maps of residual particles indicate that the internal and external mixture of particles containing different chemical nature was still preserved in the droplet phase.

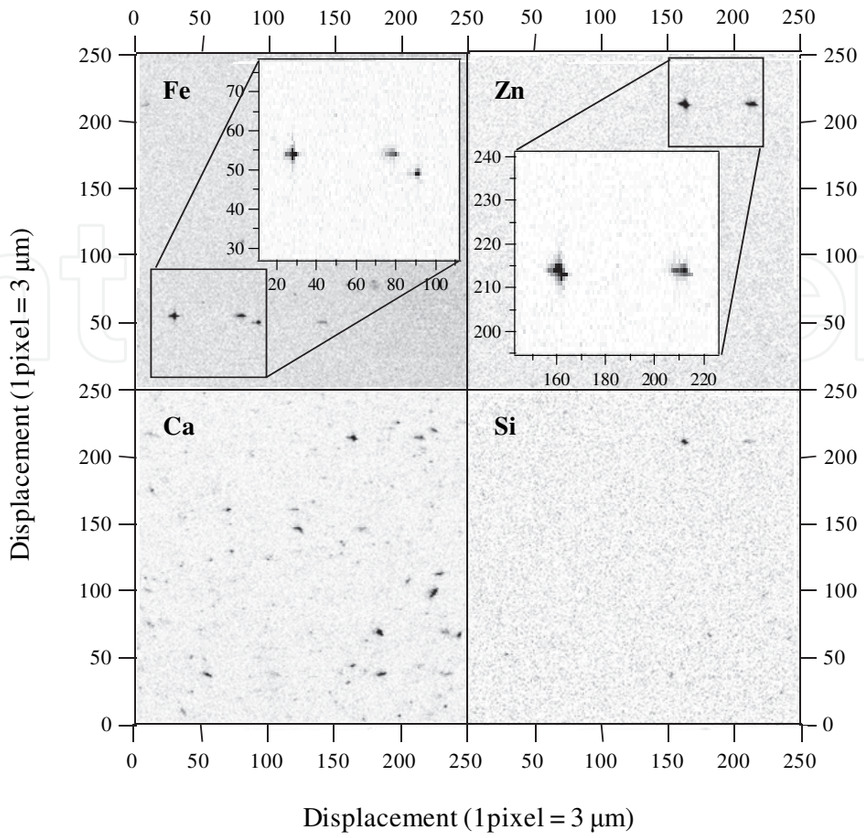

Fig. 9. XRF elemental maps of residuals in individual cloud droplets

4.2 Washout of ADS particles by raindrops

4.2.1 Sampling, handling, and analysis of individual raindrops

Sampling of size-resolved raindrops was conducted on a five-story building of Kyoto University (34.53° N; 135.48° E) during the yellow rain event in the early of April 2001. Rains started to fall in the afternoon of April 7, 2001 across southwest Japan Island as a cold front approached from the west. The front moved into east Japan late on April 7th. Total rain amount and rainfall intensity in this rainfall event were 5.0 mm and 0.8 mm/h, respectively. During sampling period the range of wind speed was 1.0~3.9 m s^{-1} generally blowing from the west. The temperature was around 19.1~19.9°C and average relative humidity was around 100%.

For the purpose of size-classified raindrop sampling, a raindrop-sampling device was employed. This raindrop-sampling device was modified from the "Guttalgor method" introduced by Tenberken and Bächmann (1996). This raindrop collector consists of a Dewar vacuum flask (Jencons Co.) filled with liquid nitrogen, five-stage stainless steel sieves with different mesh size (2.36 mm, 1.7 mm, 1.0 mm, 0.71 mm, 0.5 mm), and back-up stage. Fallen raindrops into the liquid nitrogen were frozen and they sink to lower sieves owing to their higher density. For the successful size-classification of raindrops, sampling duration time should be adjusted considering the rainfall intensity. In this study, raindrop sampling was performed for 5 minutes from the beginning rainfall. The rainfall amount for 5 minutes was 0.4 mm.

For the handling of individual raindrops without evaporation and contamination, we designed a clean air chamber system filled with cooled dry N_2 gas. After sampling, the sieves and back-up stage were pulled out from the Dewar vacuum flask and then frozen raindrops on each sieve were placed into the polyethylene vial by using a vacuum pipette. Fig. 10 shows the individual frozen raindrops collected on a mesh stage (1.7 mm mesh size) and the handling of a frozen raindrop by using a vacuum pipette. As shown in Fig. 10, the raindrops kept their spherical shape during the freezing process.

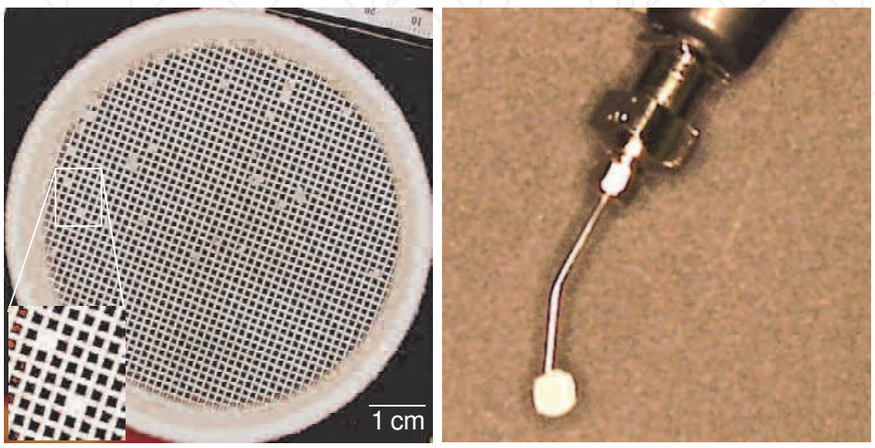

Fig. 10. Individual frozen raindrops collected on a mesh stage (1.7 mm mesh size) (left) and the handling of a frozen raindrop using a vacuum pipette (right)

To separate size-segregated raindrops into soluble and insoluble fractions, frozen raindrops were melted and then 50 μl of rainwater from each raindrop size was centrifuged under the condition of 4000 rpm for 10 min. Centrifuging method can be used to separate the solids from liquid 12). Centrifuging can be effectively used especially for the relatively small amount of liquid sample. When the insoluble particle is placed in a centrifugal field (maximum centrifugal force: 2,670 g), a force higher than gravity pulls the particle down. By centrifuging treatment, the solid insoluble particles could be deposited on a non-hole Nuclepore® film. Also 20 μl of upper soluble fraction was dropped on a non-hole Nuclepore film and then water fraction was evaporated under an infrared lamp. The solid insoluble particles and the residual material of upper solution were subsequently analyzed as the insoluble and soluble fractions, respectively. Elemental concentrations of the soluble and insoluble fractions were determined by PIXE analytical method. For the elemental quantification analysis of the individual solid particles retained in raindrops, the XRF microbeam system equipped at SPring-8 BL-37XU was applied. The analytical procedures and experimental set-up used for both analysers were mentioned earlier.

4.2.2 Replication of individual cloud droplets

Fig. 11 exhibits the variation of major elemental mass concentrations as the function of solubility and raindrop size. Since the giant raindrop, which is larger than 3.5 mm diameter, will be easily split into smaller one, the whole size range of raindrop was considered from 0.2 mm to 3.5 mm diameter. As shown in Fig. 11, every elemental concentration in both soluble and insoluble fractions is found to be strong raindrop size dependence. Though

there is the slight increase of K concentration between 1.7 mm and 2.3 mm raindrop diameter, it shows a strong decrease of every elemental concentration with increasing droplet diameter regardless of solubility. Especially S and Cl show the predominantly higher mass loading in soluble fraction. It is expected that the following several mechanisms are responsible for this raindrop size dependence of elemental concentration (Bächmann et al., 1993):

- Inside the cloud
- The scavenging of particles by CCN mechanism
- The uptake of gases
- The collision and coalescence
- Below the cloud
- The scavenging of particles by impaction, collision, and coalescence
- The uptake of gases
- Raindrop evaporation

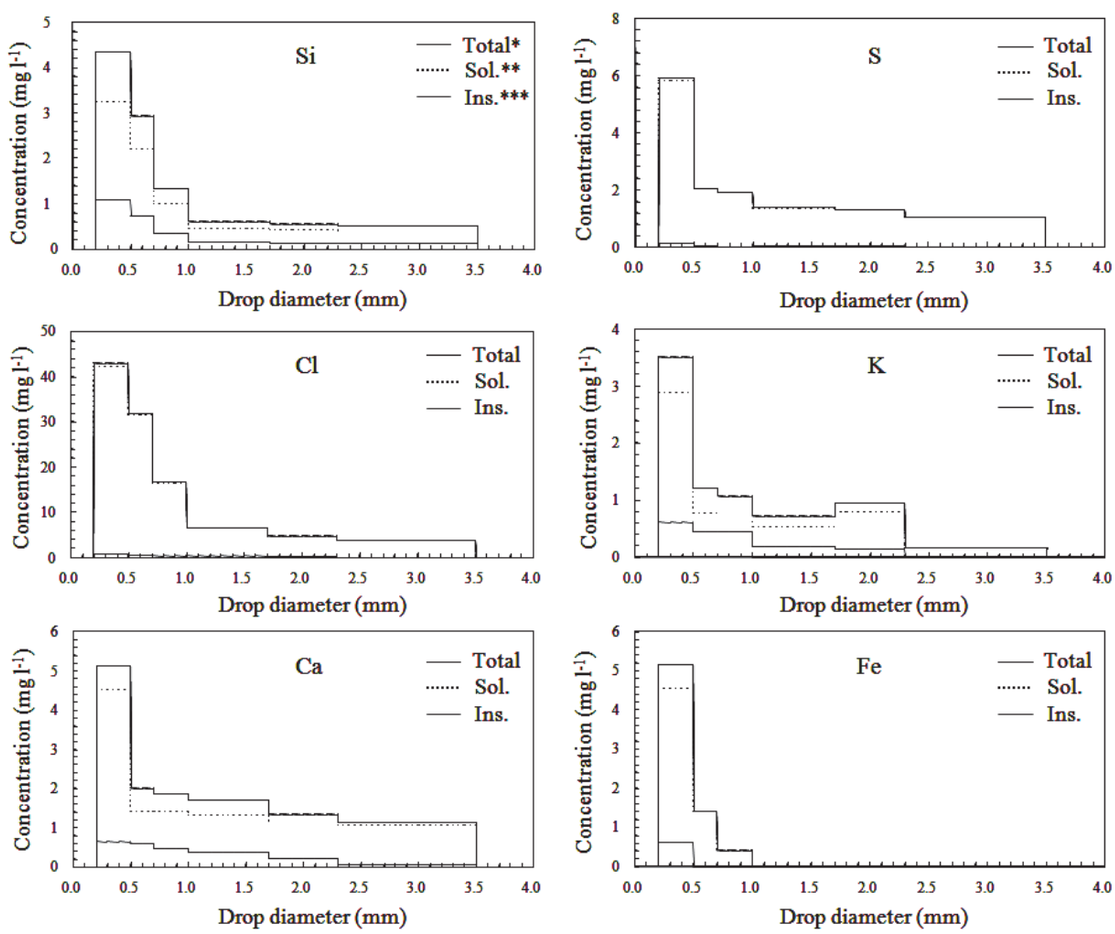

Fig. 11. The variation of major elemental masses as the function of solubility and raindrop size.
*Sum of soluble and insoluble (outer bold)
**Soluble
***Insoluble (inner bold)

Flossman (1994) stated that raindrops within the cloud or near the cloud base have nearly identical concentrations regardless of raindrop size. Moreover, according to Munger's measurement in the coastal stratus clouds (Munger et al., 1983), the continuous decreasing of component concentrations in cloud was not found. On the other hand, at the ground-based measurement in the present study, the dependence of elemental concentration on raindrop diameter was found. Therefore it is suggested that dependence of elemental concentration on drop size measured near and at the ground is only due to below cloud influences (Tenberken & Bächmann, 1996). When raindrops fall from cloud base to ground, due to below cloud scavenging of pollutants the solute concentration in raindrop will be increased. Hans and James (1998) also reported that the scavenging efficiency of pollutants by falling raindrops decreases with increasing raindrop size with the range of 0.2 mm to 4 mm diameter.
In the case of insoluble fraction, the concentration ratios of Si, K, Ca, and Fe in yellow rain (average value of size-classified raindrop samples) to those in non-yellow rain (Park, 1997) are 12.4, 11.4, 13.7, and 10.1, respectively. They also show the overwhelmingly higher ratios at soluble fraction. It is clear that the episodically yellowish rainfall shows a high load for crustal materials in both soluble and insoluble fractions.

4.2.3 Model calculation of elemental mass in size-resolved raindrops

For the purpose of comparing the measured mass concentration of each element to calculated mass concentration in size-resolved raindrop, we made an attempt to determine the each elemental mass concentration as a function of raindrop size by model calculation. The schematic of model concept is illustrated in Fig. 12. This model is a Lagrange type model that set the special coordinates as the one-dimensional vertical direction from below cloud base to ground. For model calculation, we assumed several parameters as following: the uniform distribution of aerosol particles existing in a volume swept by falling raindrops, the stable atmosphere, no diffusion by a rising air current, no evaporation and coalescence of raindrops. When the raindrop with diameter d_r falls for one second, the volume V swept by falling raindrop is described as following equation.

$$V = \frac{\pi {d_r}^2}{4} \upsilon_t \tag{1}$$

where υ_t is the terminal velocity.
When the mass concentration of particles with diameter d_p at ground is defined as $C_{p,0}$ (d_p), and the collection efficiency of raindrop with d_r for particle with diameter d_p is defined as E_0 (d_r, d_p), the mass (m) of particle (d_p) in raindrop (d_r), which falls through V for one second, can be written as following.

$$m = \frac{\pi {d_r}^2}{4} \upsilon_t \cdot C_{p,0}(d_p) \cdot E_0(d_r, d_p) \tag{2}$$

Therefore the total mass (M) of particle (d_p) in raindrop (d_r), which falls through from below cloud base to ground, can be rearranged as following equation.

$$M = \int_0^t \frac{\pi {d_r}^2}{4} \upsilon_t(h, d_r) \cdot C_p(h, d_p) \cdot E(h, d_r, d_p) dt \tag{3}$$

where $\upsilon_t(h, d_r)$ is the terminal velocity of raindrop (d_r) at height (h), $C_p(h, d_p)$ is the mass concentration of particles existing at height (h), $E(h, d_r, d_p)$ is the collection efficiency of raindrop (d_r) for particle (d_p) at height (h).

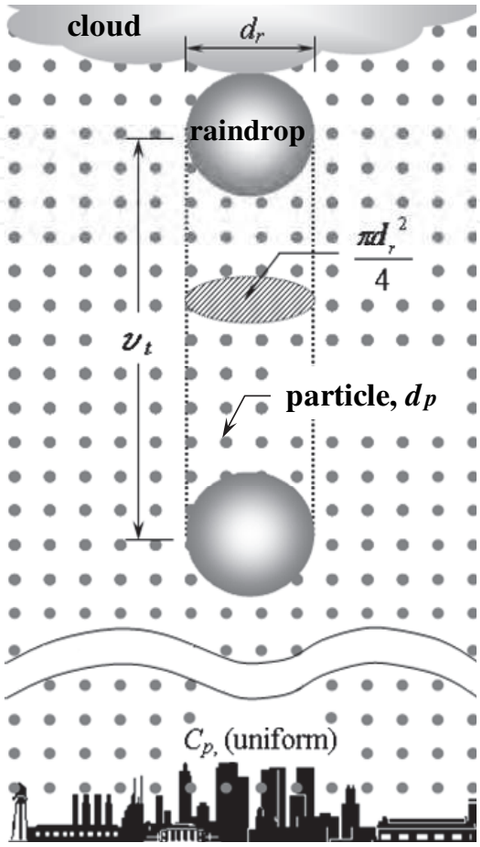

Fig. 12. Schematic of the model used for the calculating each elemental mass concentration as a function of raindrop size at ground

About the terminal velocity of raindrops (U_t, cm s^{-1}), we applied the Beard's (1976) three physically distinct flow regimes: 1) small cloud droplets, 1 μm≤d_0≤20 μm (steady wake, vanishingly small Reynolds number, 10^{-6}≤N_{Re}≤0.01), 2) large cloud droplets to small raindrops, 20 μm≤d_0≤1 mm (steady wake, low to intermediate Reynolds number, 0.01≤N_{Re}≤300), 3) small to large raindrops, 1 mm≤d_0≤7mm (unsteady wake, moderate to large Reynolds number, 300≤N_{Re}≤4000).

Though other mechanisms like diffusiophoresis, electrostatic force, and thermophoresis are comprised in particle scavenging by raindrop in the atmosphere, aerosol particles can be mainly removed through the processes of Brownian diffusion, interception, and impaction. Therefore, in the present study the particle collection efficiency (E) of raindrops including Brownian diffusion (E_{dif}), interception (E_{int}), inertial impaction processes (E_{imp}), and the combined with these three particle scavenging coefficients (E_{com}) as a function of raindrop size were calculated. In order to formulate a correlation for E based on dimensional analysis, the parameters that influence E must be identify (Seinfeld & Pandis, 1998). The parameters are several variables such as volume of raindrop (f, cm^3), scale height (h, m), rain intensity

(I, mm h^{-1}), total number concentration of raindrop (N, m^{-3}), raindrop radius (r_r, μm), Reynolds number (Re), critical Stokes number (S^*), raindrop terminal settling velocity (υ_t, cm s^{-1}), rainwater concentration in the atmosphere (W, mg m^{-3}), vertical distance from the cloud base (z, m), dynamic viscosity of air (μ_a, Pa·s), particle diffusivity (D_p, cm s^{-2}), and dynamic viscosity of water (μ_r, Pa·s). Based on E_{dif}, E_{int}, and E_{imp}, Strauss (1975) proposed the following E_{com} equation that fits experimental data:

$$E_{com}=1-(1-E_{dif})\cdot(1-E_{int})\cdot(1-E_{imp}) \tag{4}$$

In this work, the following E_{dif}, E_{int}, and E_{imp} proposed by Slinn and Hales (1971) were applied.

$$E_{dif}=\frac{4}{Re\cdot Sc}\left(1+0.4Re^{1/2}Sc^{1/3}\right) \tag{5}$$

$$E_{int}=4\frac{r_p}{r_r}\left(\frac{\mu_a}{\mu_r}+(1+2Re^{1/2})\frac{r_p}{r_r}\right) \tag{6}$$

$$E_{imp}=\left(\frac{St-S^*}{St-S^*+2/3}\right)^{3/2} \tag{7}$$

where Re is the Reynolds number of raindrop based on its radius ($(r_r\,\upsilon_t\,\rho_a)/\mu_a$). Sc is the Schmidt number of collected particle ($\mu_a/\rho_a\cdot D_p$). St is the Stokes number of collected particle ($(2C\,\rho_p\,r_p\,\upsilon_t)/(9\mu_a\,r_r)$), C is the Cunningham slip factor, ρ_p is the particle density kg m^{-3}. S^* is the critical Stokes number ($(1.2+(1/12)\ln(1+Re))/(1+\ln(1+Re))$).

In the present study, six major components (Si, S, Cl, K, Ca, Fe) were the target of model calculation. To get the elemental mass information at atmosphere, concurrently with the raindrop sampling, the collection of size-classified particles by LPAI (Dylec, LP-20) was conducted at the same sampling site. The detailed specifications of LPAI were described previous study (Ma et al., 2004a).

The PIXE analysis results of soluble and insoluble fractions for the size-segregated ambient particles were applied to the calculation of mass concentrations of **six** elements as a function of raindrop size. The elemental mass concentration at height (h) can be given by

$$C(h)=C_g(0)\exp\left(-\frac{h}{H}\right) \tag{8}$$

where C(h) is the atmospheric concentration of target component at height (h). $C_g(0)$ is the atmospheric concentration of target component at ground. H is the scale height, 900 m.

The height of Mt. Hiei (848 m) which is located close to our raindrop sampling site was a barometer of the height of cloud above ground level because the widely distributed cloud was suspended right above the summit of Mt. Hiei.

The calculated mass concentrations of six elements as a function of raindrop size are plotted with measured results in Fig. 13. Raindrops were fractionated into size class 0.2-0.5, 0.5-0.7, 0.7-1.0, 1.0-1.7, 1.7-2.3, and 2.3-3.5 mm diameter. The phenomenon of the continuous decreasing of elemental mass concentration with increasing raindrop size was shown in both calculated and measured results.

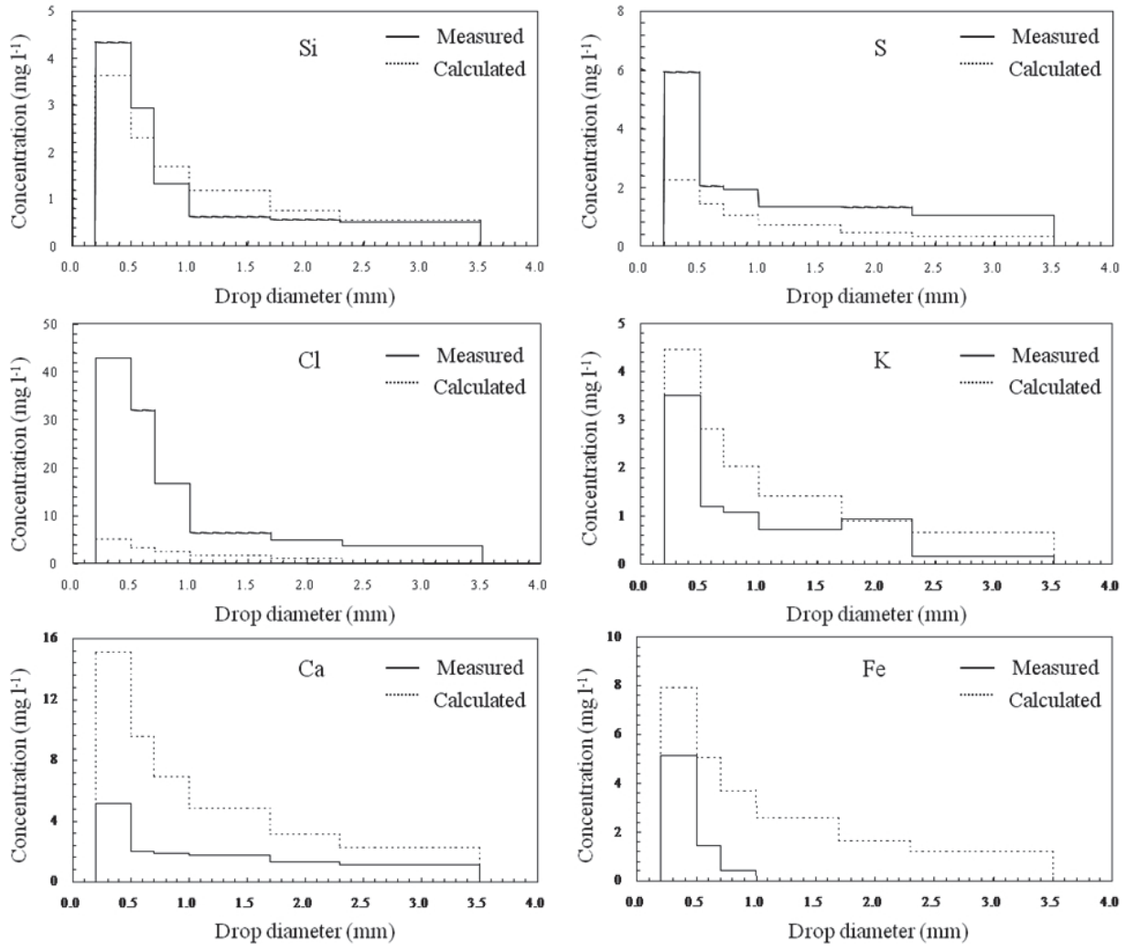

Fig. 13. The plotting of calculated vs. measured mass concentrations for six major elements as a function of raindrop size

A comparatively good agreement was obtained between measured and calculated results for Si, S, and K. However, the calculated Cl mass concentration was considerably under estimated compared with measured results. Whereas, in the case of Ca and Fe, the calculated mass concentrations over estimated. One of the reasons for these discrepancies between measured and calculated levels might be the inhomogeneous particle distribution from below cloud base to ground. Because the physicochemical properties of Asian dust particles will be exceedingly variable according the transport situation, local emission sources, and atmosphere conditions. Furthermore, the long sampling duration time (24 hours) for ambient particle collection can obscure the particle-to-particle composition variations because the particle composition may be altered due to condensation or evaporation of volatile compounds, or chemical reactions. Therefore spatial and temporal inhomogeneities in air mass might lead to disagreement between calculated and measured results. From this point of view, the sampling of atmospheric particles must be done with good time-resolved sampling duration. The continuous sampling of size-resolved raindrop as a function of rainfall amount with the detailed size-classification of fine fraction raindrop with diameter smaller than 0.5 mm is also desirable.

4.2.4 Chemical components of individual particles retained raindrops

By irradiation of the XRF microbeam, it was possible to reconstruct individual particles retained raindrops as elemental maps. Fig. 14 draws the example XRF elemental maps for Fe, Cl, Si, and Ca in individual particles retained in raindrops (1.7 mm<Rd<2.36 mm). These visualized elemental maps for four kinds elements enable us not only to estimate the chemical mixing state of raindrop residual particles, but also to presume the particle scavenging of raindrops. For example, some particles indicate the chemical mixing state with soil derived components and Cl, while others consist of only crustal components. Consequently, from these four kinds of XRF images replayed corresponding to individual residual particles in raindrops, we can simply fractionate the visualized particle images into several groups.

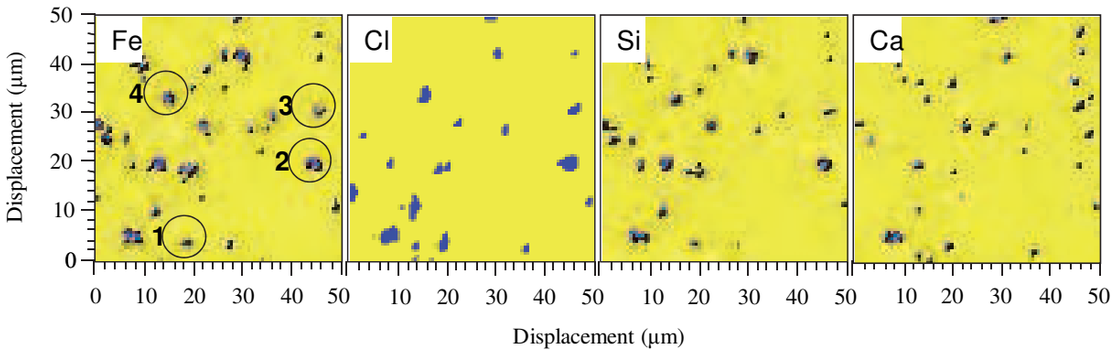

Fig. 14. XRF images of Fe, Cl, Si, and Ca in individual particles retained in raindrops (1.7< Rd <2.36 mm)

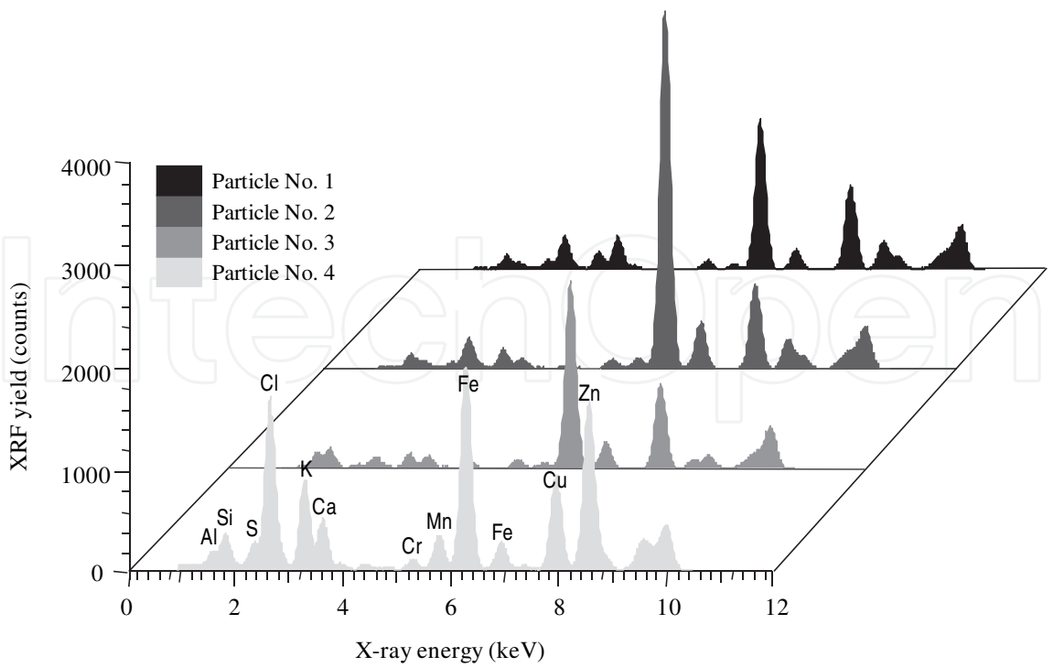

Fig. 15. XRF spectra for four particles indicated in Fig. 14. XRF counts were counted for 100 seconds

The XRF spectra for four particles indicated in Fig. 14 are plotted in Fig. 15. It was possible to resolve the multiple elemental peaks corresponding to X-ray energy of XRF spectra. The XRF count for every element shows the particle-to-particle variation. Among the soil-originated components, especially Fe shows high XRF counts. Several minor trace elements like Cr, Mn, and Cu are also coexisted with crustal elements. However, the XRF peak for Cu was overestimated because the sample holder of our XRF analytical system contains Cu. The elemental mass concentration (mg l^{-1}) for multielement can be quantitatively calculated by X-ray energy and count of each element.

5. Conclusion

As the source of ADS particles, the sands at four different desert areas were to be the target of bulk and single analyses by means of PIXE and SR-XRF analyses, respectively. The physical properties of desert sands like morphology, color, and size were basically determined. Also the chemical characteristics of bulk sands of each desert were specified as the relative elemental ratio. The XRF elemental maps and spectra for a point on individual sands allow us to understand the nature of individual sands. Consequently, the physicochemical properties of desert sands obtained from this study can be helpful to understand what kinds of man-made pollutants and sea-salts are incorporated into natural ADS particles.

By a combination of two different detector systems of micro-PIXE, a broad detection range of elements including Na, Mg, and Al was successively realized. The well drawn elemental spectra and maps from this novel attempt enabled us to visually classify individual ADS particles. It was also possible to sufficiently interpret the mixing state of individual ADS particles with sea-salts, especially portion-to-portion dissimilarity of chemical state in individual ADS particles. In addition to this, the detailed information of elemental micro distribution obtained from the scanning of microbeam with a 1-2 μm beam diameter in and/or on an ADS particle helped us presume the aging processes of ADS particles both in ambient and in-cloud. The relative number fraction of chemically transformed particle type in the size-classified particles collected during ADS event indicates that the chemical mixing states of individual ADS particles are strongly dependent on particle size.

The significant distribution of crustal components on the elemental maps reconstructed by XRF microprobe analysis indicates that a large number of crustal particles were incorporated into cloud droplets during their long-range transport. In other words, ADS particles were effectively scavenged by rain out mechanisms. Elemental concentrations in both soluble and insoluble fractions were found to be strong raindrop size dependence showing a sharp decrease of concentration with increasing raindrop size. Even though the tendency of the continuous decreasing of elemental mass concentration across the raindrop size spectrum was also shown in the model calculation, to improve the results of modeling calculation, the sampling of atmospheric particles with good time-resolved sampling duration is desirable. By a combination of XRF microbeam method, the individual particles retained in size-resolved raindrops were successfully characterized. Though the in-cloud scavenging of ADS particles is also expected, the results of our study make certain of the truth that the wet removal processes is one of final dissipation mechanisms of ADS particles.

6. Acknowledgments

The synchrotron radiation experiments were performed at the SPring-8 with approval of the Japan Synchrotron Radiation Research Institute (JASRI) (Proposal No. 2002B0395-NOS-np, 2002A4029-LM-np). The authors gratefully acknowledge Professor S. Tohno at Graduate School of Energy Science, Kyoto University and Professor S. Hayakawa at Graduate School of Engineering, Hiroshima University for their analytical support. The author wishes to express thanks to all the members, especially Mr. T. Sakai, in the Advanced radiation technology center, Japan Atomic Energy Research Institute for their help of micro-PIXE analysis. The author also gratefully acknowledges Professor M. Kasahara at Institute of Science and Technology Research, Chubu University for his planning and arrangement of micro-PIXE experiment for a long period.

7. References

Avila, A. & Rodà, F.: Red rains as major contributors of nutrients and alkalinity to terrestrial ecosystems at Montseny (NE Spain). *Orsis*, 6, 215-218 (1991)

Bächmann, K.; Haag, I. & Roder, A. (1993). A field study to determine the chemical content of individual raindrops as a function of their size. *Atmospheric Environment*, 27A, 1951-1958

Baez, A.P.; Belmont, R. & Padilla, H. (1995). Measurements of formaldehyde and acetaldehyde in the atmosphere of Mexico City. *Environmental Pollution*, 89, 163-171

Beard, K.V. (1976). Terminal velocity and shape of cloud and precipitation drops. *Journal of Atmospheric Science*, 33, 851-864

Berganetti, G.; Gomes, L.; Coude-Gaussen, G., Rognon, P. & Le Costumer, M. (1989). Present transport and deposition patterns of African dusts to the North-Western Mediterranean. *Journal of Geophysical Research*, 94 D12, 14855-14864

Braaten, D.A. & Cahill, T.A. (1986) Size and composition Asian dust transported to Hawaii. *Atmospheric Environment*, 20, 1105-1109.

Chate, D.M. & Kamra, A.K. (1997). Collection efficiencies of large water drops collecting aerosol particles of various densities. *Atmospheric Environment*, 31, 1631-1635

Darzi, M.D. & Winchester, W. (1982) Aerosol characteristics at Mauna Loa observatory, Hawaii, after east Asia dust storm episodes. *Journal of Geophysical Research*, 87, 1251-1258.

Desboeufs K.V.; Losno, R. & Colin, J.L. (2001) Factors influencing aerosol solubility during cloud processes. *Atmospheric Environment*, 35, 3529-3537.

Duce R.A.; Unni, C.K.; Ray, B.J.; Prospere, J.M. & Merrill, J.T. (1980) Long-range atmospheric transport of soil dust from Asia to the tropical north Pacific: Temporal variability. *Science*, 209, 1522-1524.

Flossman, A.I. (1994). A 2-D spectral model simulation of the scavenging of gaseous and particulate sulfate by a warm marine cloud. *Atmospheric Research*, 32, 233-248

Hallberg, A.; Wobrock, W.; Flossmann, A.I.; Bower, K.N.; Noone, K.J.; Wiedensohler, A.; Hansson, H. C.; Wendisch, M.; Berner, A.; Kruisz, C.; LAJ, P.; Facchini, M. C.; Fuzzi, S. & Arends, B.B. (1997). Microphysics of clouds: Model vs measurements. *Atmospheric Environment*, 31, 2453-2462

Hans, R.P. & James, D.K. (1998). Microphysics of clouds and precipitation. *Atmospheric and Oceanic Sciences Library*, 18, 24-30

Hayakawa, S. (2000) X-ray fluorescence method for trace analysis and imaging. Journal of *Japanese Synchrotron Radiation Research*, 13, 313-318. (in Japanese)

Hayakawa, S.; Ikuta, N.; Suzuki, M.; Wakatsuki, M. & Hirokawa, T. (2001) Generation of an X-ray microbeam for spectromicroscopy at SPring-8 BL39XU. *Journal of Synchrotron Radiation*, 8, 328-330.

Husar, R.B.; Tratt, D.M.; Schichtel, B.A.; Falke, S.R.; Li, F.; Jaffe, D.; Gassó, S.; Gill, T.; Laulainen, N.S.; Lu, F.; Reheis, M.C.; Chun, Y.; Westphal, D.; Holben, B.N.; Gueymard, C.; McKendry, I.; Kuring, N.; Feldman, G.C.; McClain, C.; Frouin, R.J.; Merrill, J.; DuBois, D.; Vignola, F.; Murayama, T.; Nickovic, S.; Wilson, W.E.; Sassen, K.; Sugimoto, N. & Malm, W.C. (2001) The Asian Dust Events of April 1998. *Journal of geophysical research atmospheres*, 106 (D16), 18317-18330.

Hwang, H.J.; Kim, H.K. & Ro, C.U. (2008) Single-particle characterization of aerosol samples collected before and during an Asian dust storm in Chuncheon, Korea. *Atmospheric Environment*, 42, 8738–8746.

Iwasaka, Y.; Yamamoto, M.; Imasu, R. & Ono, A. (1988) Transport of Asian dust (KOSA) particles: importance of weak KOSA events on the geochemical cycle of soil particles. *Tellus*, 40B, 494-503.

Johansson, S.A.E. & Campbell, J.L. (1988) *PIXE*: A novel technique for elemental analysis. New York: John Wiley and Sons, pp.134-140.

Lafon, S.; Rajot, J.-J.; Alfaro, S.C. & Gaudichet, A. (2004) Quantification of iron oxides in desert aerosol. *Atmospheric Environment*, 38, 1211-1218.

Li, R.; Liu, Y. & Zhang, K. (2007) Plant species diversity of wetland ecosystem in an arid and semi-arid region in northwest China. *Frontiers of Forestry in China*, 2(3), 284-290.

Ma, C.-J. (2001). New approaches for characterization of atmospheric particles and acid precipitation, Ph. D. dissertation, Kyoto University

Ma, C.-J.; Kasahara, M.; Hwang, K.C.; Choi, K.C.; Choi, S.B. & Lee, J.J. (2000) Physicochemical characteristics of single Asian dust storm particles. *Journal of Korean Society for Atmospheric Environment*, 16 E, 29-38.

Ma, C.J.; Kasahara, M. & Tohno, S., 2001. A new approach for characterization of single raindrops. *Water, Air and Soil Pollution*, 130, 1601-1606.

Ma, C.-J.; Kasahara, M. & Tohno, S. (2002). Application of PIXE to characterization of size-segregated single raindrops. *International Journal of PIXE*, 12, 7-18

Ma, C.-J.; Kasahara, M.; Tohno, S. & Kamiya, T. (2001). A new approach for characterization of single raindrops, *Water, Air, and Soil Pollution*, 130, 1601-1606

Ma, C.-J.; Kasahara, M.; Tohno, S. & Kim, K.-H. (2008) Physicochemical properties of Asian dust sources. *Asian Journal of Atmospheric Environment*, 2-1, 26-33.

Ma, C.-J. & Kim, K.-H. (2008) A combination of size-resolved particle samplers and XRF microprobe technique for single particle study. *Atmospheric Environment*, 42, 7022-7026.

Ma, C.-J.; Oki, Y.; Tohno, S. & Kasahara, M. (2004a) Assessment of wintertime atmospheric pollutants in an urban area of Kansai, Japan. *Atmospheric Environment*, 38, 2939-2949.

Ma, C.-J.; Tohno, S.; Kasahara, M. & Hayakawa, S. (2004b) Properties of the size-resolved and individual cloud droplets collected in the western Japan during Asian dust storm event. *Atmospheric Environment*, 38, 4519-4529.

Ma, C.-J.; Tohno, S.; Kasahara, M. & Hayakawa, S. (2004c) Properties of individual Asian dust storm particles collected at Kosan, Korea during ACE-Asia. *Atmospheric Environment*, 38, 1133-1143.

Mason, B. (1966) *Principles of Geochemistry*, 3rd edn. Wiley, New York.

Munger, J.W.; Jacob D.J.; Waldman J.M. & Hoffmann M.R. (1983). Fogwater chemistry in an urban atmosphere. *Journal of Geophysical Research*, 88, 5109-5123

Nishikawa, M.; Hao, Q. & Morita, M. (2000) Preparation and Evaluation of Certified Reference Materials for Asian Mineral Dust. *Global Journal of Environmental Research*, 4, 103-113.

Nishikawa, M. & Kanamori, S. (1991) Chemical composition of Kosa aerosol (yellow sand dust) collected in Japan. *Analytical Science*, 7, 1127-1130.

Park, J.H. (1997). Study of physicochemical properties of atmospheric particles and their scavenging. Ph. D. dissertation, Kyoto University (In Japanese).

Rodà, F.; Bellot, J.; Avila, A.; Escarré, A.; Piñol, J. & Terradas, J. (1993). Sahara dust and the atmospheric inputs of elements and alkalinity to Mediterranean ecosystems. *Water, Air, and Soil Pollution*, 66, 277-288

Sakai, T.; Oikawa, M. & Sato, T. (2005) External Scanning Proton Microprobe –A New Method for In-Air Elemental Analysis. *Journal of Nuclear and Radiochemical Sciences*, 6(1), 69-71.

Seinfeld, J.H. & Pandis, S.N. (1998). *Atmospheric Chemistry and Physics*, pp.1003-1013, John Wiley & Sons Press, New York

Slinn, W. G.N. & Hales, J.M. (1971). A revaluation of the role of thermophoresis as a mechanism in and below cloud scavenging. *Journal of Atmospheric Science*, 28, 1465-1471

Song, C.H. & Carmichael, G.R. (1999) The aging process of naturally emitted aerosol (sea-salt and mineral aerosol) during long range transport. *Atmospheric Environment*, 33, 2203-2218.

Song, M.; Lee, M.; Moon, K.J.; Han, J.S.; Kim, K.R. & Lee, G. (2006) Chemical characteristics of fine aerosols during ABC-EAREX2005. *Journal of Korean Society for Atmospheric Environment,* 22, 604-613.

Strauss, W. (1975). *Industrial gas cleaning*. pp. 293-3005, Pergamon Press, New York

Tenberken, B. & Bächmann, K. (1996). Analysis of individual raindrops by capillary zone electrophoresis. *Journal of Chromatograph A*, 755, 121-126

The standards of China loess and Simulated Asian mineral dust (1998). Sino-Japan Friendship Centre for Environmental Protection (SJC), Available from http://www.china-epc.cn/ japan/index_e.htm

Zhang, D. & Iwasaka, Y. (1998) Morphology and chemical composition of individual dust particles collected over Wakasa bay, Japan. *Journal of Aerosol Sciene*, 29, S217-S218.

Zhang, D. & Iwasaka, Y. (2004) Size change of Asian dust particles caused by sea salt interaction: Measurements in southwestern Japan. *Journal of Geophysical Research*, 31, L15102, doi:10.1029/2004GL020087.

Zhang, D.; Iwasaka, Y.; Shi, G.; Zang, J.; Matsuki, A. & Trochkine, D. (2003) Mixture state and size of Asian dust particles collected at southwestern Japan in spring 2000. *Journal of Geophysical Research*, 108, 4760, doi:10.1029/2003JD003869.

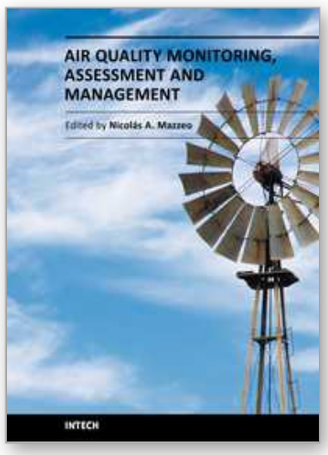

Air Quality Monitoring, Assessment and Management

Edited by Dr. Nicolas Mazzeo

ISBN 978-953-307-317-0
Hard cover, 378 pages
Publisher InTech
Published online 08, July, 2011
Published in print edition July, 2011

Human beings need to breathe oxygen diluted in certain quantity of inert gas for living. In the atmosphere, there is a gas mixture of, mainly, oxygen and nitrogen, in appropriate proportions. However, the air also contains other gases, vapours and aerosols that humans incorporate when breathing and whose composition and concentration vary spatially. Some of these are physiologically inert. Air pollution has become a problem of major concern in the last few decades as it has caused negative effects on human health, nature and properties. This book presents the results of research studies carried out by international researchers in seventeen chapters which can be grouped into two main sections: a) air quality monitoring and b) air quality assessment and management, and serves as a source of material for all those involved in the field, whether as a student, scientific researcher, industrialist, consultant, or government agency with responsibility in this area.

InTech Europe
University Campus STeP Ri
Slavka Krautzeka 83/A
51000 Rijeka, Croatia
Phone: +385 (51) 770 447
Fax: +385 (51) 686 166
www.intechopen.com

InTech China
Unit 405, Office Block, Hotel Equatorial Shanghai
No.65, Yan An Road (West), Shanghai, 200040, China
中国上海市延安西路65号上海国际贵都大饭店办公楼405单元
Phone: +86-21-62489820
Fax: +86-21-62489821

IntechOpen